Optical Materials 60 (2016) 431–437

Contents lists available at ScienceDirect

Optical Materials

journal homepage: www.elsevier.com/locate/optmat

Comparative study of the Mn^{4+} $^2E \rightarrow {}^4A_2$ luminescence in isostructural $RE_2Sn_2O_7$:Mn^{4+} pyrochlores ($RE^{3+} = Y^{3+}$, Lu^{3+} or Gd^{3+})

Tim Senden*, Fréderique T.H. Broers, Andries Meijerink

Condensed Matter and Interfaces, Debye Institute for Nanomaterials Science, Utrecht University, P.O. Box 80 000, 3508 TA, Utrecht, The Netherlands

ARTICLE INFO

Article history:
Received 24 August 2016
Accepted 24 August 2016

Keywords:
Mn^{4+}
Pyrochlore
^2E level energy
Vibronic structure
Temperature quenching

ABSTRACT

Red emitting Mn^{4+}-doped crystalline materials have potential for application in light emitting devices and therefore it is important to understand how the optical properties of Mn^{4+} are influenced by the host lattice the Mn^{4+} ions are situated in. In this work we investigate the effect of the host cations in the second coordination sphere on the Mn^{4+} emission by studying the luminescence of Mn^{4+} ions doped into three isostructural rare earth (RE) stannate $RE_2Sn_2O_7$ pyrochlores ($RE^{3+} = Y^{3+}$, Lu^{3+} or Gd^{3+}). It is found that the energies of the Mn^{4+} $^4T_1$ and $^4T_2$ states significantly increase with decreasing Mn^{4+}-O^{2-} distance, whereas the energy of the ^2E level shows a small shift to higher energies from $RE^{3+} = Gd^{3+}$ to Lu^{3+} to Y^{3+}. The observed trend for the ^2E level energy is not related to the size of the RE^{3+} ion and is not in line with theoretical calculations reported previously. Low temperature emission spectra of the $RE_2Sn_2O_7$:Mn^{4+} phosphors reveal that only asymmetrical vibronic modes couple to the $^2E \rightarrow {}^4A_2$ transition and furthermore show there is significant and unexpected local disorder for Mn^{4+} in $Gd_2Sn_2O_7$ that is not observed for Mn^{4+} in the other hosts. Photoluminescence decay measurements demonstrate that the luminescence of $RE_2Sn_2O_7$:Mn^{4+} is strongly quenched below room temperature which is assigned to non-radiative relaxation via a low-lying $O^{2-} \rightarrow Mn^{4+}$ charge-transfer state.

1. Introduction

Crystalline materials doped with Mn^{4+} ions ($3d^3$ electronic configuration) show narrow red line luminescence and are therefore interesting for applications in e.g. the lighting industry. The efficient luminescent Mn^{4+}-activated magnesium fluorogermanate is commercially used in high color rendering fluorescent lamps and high pressure mercury vapor lamps [1,2]. Furthermore, Mn^{4+}-doped fluorides and oxides can find application as red-emitting phosphors in warm-white LED devices [3–5]. Additionally, Mn^{4+}-doped materials have potential for use in holographic recording, optical data storage [6,7], thermoluminescence dosimetry [8] and as afterglow materials [9].

Because of the many potential applications, the optical properties of Mn^{4+} have been investigated for a wide variety of host lattices [3,10–12]. The practical use of Mn^{4+}-doped materials benefits from a better understanding of general relations between host lattice properties and the optical properties of the Mn^{4+} ions. For example, for lighting applications it is important to understand how the energies of the different Mn^{4+} excited states (see Fig. 2a) are influenced by the host lattice composition and Mn^{4+}-ligand distance. General studies on the spectroscopic behavior of Mn^{4+} ions in solids are however limited [10,12]. A relation has been observed between the Mn^{4+}-ligand distance and the crystal field splitting 10 Dq [13,14]. A higher crystal field splitting for shorter Mn^{4+}-ligand distances causes that the $^4T_2$ and $^4T_1$ excited states shift to higher energies when Mn^{4+} substitutes on a smaller lattice site. Furthermore, it has been found that substitution of cations in the second coordination sphere also affects the crystal field splitting [13,15].

Important for applications is the energy of the emitting ^2E level. This energy is not strongly influenced by the crystal field and is largely determined by the local covalency. In their recent work Srivastava and Brik defined a new parameter β_1 for covalency based on both the *B* and *C* Racah parameters [10]. More electronegative ligands (such as F^-) shift the ^2E emission to higher energy. The cations in the second coordination sphere also affect the energy of the ^2E level. For example, in the M_2SiF_6 (M = Na, K, Rb and Cs) compounds the zero-phonon line of the $^2E \rightarrow {}^4A_2$ emission shifts to higher energies from 16,033 cm^{-1} for M = Cs to 16,082 cm^{-1} for

* Corresponding author.
E-mail address: t.senden@uu.nl (T. Senden).

http://dx.doi.org/10.1016/j.optmat.2016.08.024
0925-3467/

M = Rb and then from 16,117 cm^{-1} for M = K to 16,230 cm^{-1} for M = Na [16–19]. To get more insight in the role of cations in the second coordination sphere on the position of the Mn^{4+} $^2E \rightarrow {}^4A_2$ emission, here we present a comparative study of the luminescence of Mn^{4+} ions doped into three different rare earth (RE) stannate $RE_2Sn_2O_7$ pyrochlores (RE^{3+} = Y^{3+}, Lu^{3+} or Gd^{3+}). In addition to investigating the positions of the energy levels, the vibronic structure and temperature quenching of the luminescence is reported for Mn^{4+} in the three hosts.

Photoluminescence (PL) excitation spectra of the Mn^{4+} $^4A_2 \rightarrow {}^4T_1$ and $^4A_2 \rightarrow {}^4T_2$ transitions for $RE_2Sn_2O_7$:Mn^{4+} (RE^{3+} = Y^{3+}, Lu^{3+} or Gd^{3+}) were recently reported by Srivastava et al. [13] to map the variation in the crystal field strength. However, in Ref. [13] the properties of the Mn^{4+} $^2E \rightarrow {}^4A_2$ luminescence, e.g. the vibronic structure, energy shift and temperature quenching, were not investigated. The thermal quenching behavior is very important for application in white LEDs, as these normally operate at temperatures between 100 and 200 °C. Furthermore, the vibronic structure of the $^2E \rightarrow {}^4A_2$ luminescence reveals the local symmetry of the Mn^{4+} ion and shows which vibronic modes couple to the parity- and spin-forbidden $^2E \rightarrow {}^4A_2$ transition. Therefore, in this work we study and compare the electronic and vibronic structure in luminescence spectra of Mn^{4+} in $RE_2Sn_2O_7$ (RE^{3+} = Y^{3+}, Lu^{3+} or Gd^{3+}) by measuring PL emission and excitation spectra at cryogenic temperatures. Additionally, we measure the PL decay of the Mn^{4+} ^2E state as a function of temperature and thereby investigate the thermal quenching behavior for Mn^{4+} in $RE_2Sn_2O_7$. It is observed that the energies of the Mn^{4+} $^4T_1$ and $^4T_2$ states significantly increase with decreasing Mn^{4+}-O^{2-} distance, whereas the low temperature measurements reveal a small energy shift for the ^2E state that is not consistent with recent calculations for the ^2E level of Mn^{4+} in these hosts. The vibronic structure of the Mn^{4+} luminescence reveals which vibrational modes couple to the $^2E \rightarrow {}^4A_2$ transition. Large inhomogeneous broadening shows there is significant and unexpected local disorder for Mn^{4+} in $Gd_2Sn_2O_7$ that is not observed for Mn^{4+} in the other hosts. Finally, the PL decay measurements demonstrate that the luminescence of $RE_2Sn_2O_7$:Mn^{4+} is strongly quenched below room temperature with a lower quenching temperature for Mn^{4+} in the Gd-host. The quenching is assigned to relaxation via a low-lying $O^{2-} \rightarrow Mn^{4+}$ charge-transfer state.

2. Materials and methods

Microcrystalline powders of $RE_2Sn_2O_7$ (RE^{3+} = Y^{3+}, Lu^{3+} or Gd^{3+}) doped with 1% of Mn^{4+} ions were synthesized according to the method of Srivastava et al. [13]. The starting materials used for the syntheses were Y_2O_3 (Sigma-Aldrich, 99,99%), Lu_2O_3 (Chem-PUR, 99,9%), Gd_2O_3 (Highways International, 99,999%), SnO_2 (Fisher Scientific, 99,9%) and $MnCO_3$ (Sigma-Aldrich, ≥99,9%). The powders were synthesized by mixing and grinding stoichiometric amounts of the starting materials with a pestle in a mortar and heating for 5 h in a covered alumina crucible at 1000 °C in air. Next, the samples were ground a second time and heated for 10 h in a covered alumina crucible at 1400 °C in air. The phase purity and crystal structure of the obtained light yellow-brown powders were investigated by powder x-ray diffraction (XRD). XRD patterns were recorded with a Philips PW1729 x-ray diffractometer using CuK_α radiation.

Photoluminescence (PL) spectra and decay curves of the samples were measured using an Edinburgh Instruments FLS920 fluorescence spectrometer equipped with a single 0.22 m excitation and emission monochromator. For recording excitation and emission spectra, we used a 450 W Xe lamp as excitation source and a Hamamatsu R928 photomultiplier tube (PMT) for detection of emission. For PL decay measurements we used an optical parametric oscillator (OPO) system (Opotek HE 355 II) pumped by the third harmonic of a Nd:YAG laser as excitation source. This OPO system offers a continuously tunable optical range from 410 to 2400 nm, with a pulse width of 10 ns. For the PL decay measurements, the OPO system was set at λ_{exc} = 470 nm ($Y_2Sn_2O_7$:Mn^{4+}) or 485 nm ($Gd_2Sn_2O_7$:Mn^{4+}), with a repetition rate of 10 Hz. The PL decay was recorded with a Hamamatsu R928 PMT in combination with the multi-channel scaling (MCS) option available on the Edinburgh Instruments FLS920 fluorescence spectrometer. For PL measurements down to 4 K, the samples were cooled in an Oxford Instruments liquid helium flow cryostat. Diffuse reflection spectra were measured with a Perkin-Elmer 950 UV/VIS/NIR absorption spectrometer.

3. Results and discussion

3.1. Structural characterization

The crystal structure and phase purity of the $RE_2Sn_2O_7$:Mn^{4+} (1%) phosphors were investigated by powder x-ray diffraction (XRD), as is shown in Fig. 1. The XRD patterns are in excellent agreement with reference patterns of the $RE_2Sn_2O_7$ pyrochlores. No traces of impurity crystal phases are observed. The diffraction lines of the $RE_2Sn_2O_7$:Mn^{4+} (1%) phosphors shift to higher angles with decreasing ionic radius of the RE^{3+} ion, as the unit cell volume of the $RE_2Sn_2O_7$ pyrochlore reduces when the size of the RE^{3+} ion decreases. Consequently, the Mn^{4+}-O^{2-} (Sn^{4+}-O^{2-}) distance in the MnO_6 octahedron is shorter when the ionic radius of the RE^{3+} ion is smaller, as is shown in Table 1 [20,21].

3.2. Electronic structure for Mn^{4+}

In a crystal field the free ion Mn^{4+} ($3d^3$) LS terms split into a number of sublevels, depending on the crystal field strength and

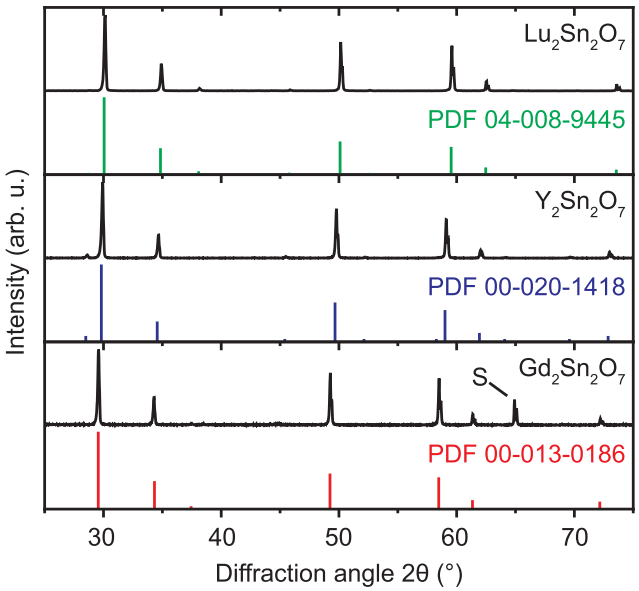

Fig. 1. – X-ray diffraction (XRD) patterns to test the phase purity of the $RE_2Sn_2O_7$:Mn^{4+} phosphors. The x-ray diffraction patterns of $RE_2Sn_2O_7$:Mn^{4+} (1%) (RE^{3+} = Y^{3+}, Lu^{3+} or Gd^{3+}) are in excellent agreement with the reference patterns of $Gd_2Sn_2O_7$ (PDF-00-013-0186, red), $Y_2Sn_2O_7$ (PDF-00-020-1418, blue) and $Lu_2Sn_2O_7$ (PDF-04-008-9445, green). The **S** marks a diffraction line originating from the aluminum sample holder. (For interpretation of the references to color in this figure legend, the reader is referred to the web version of this article.)

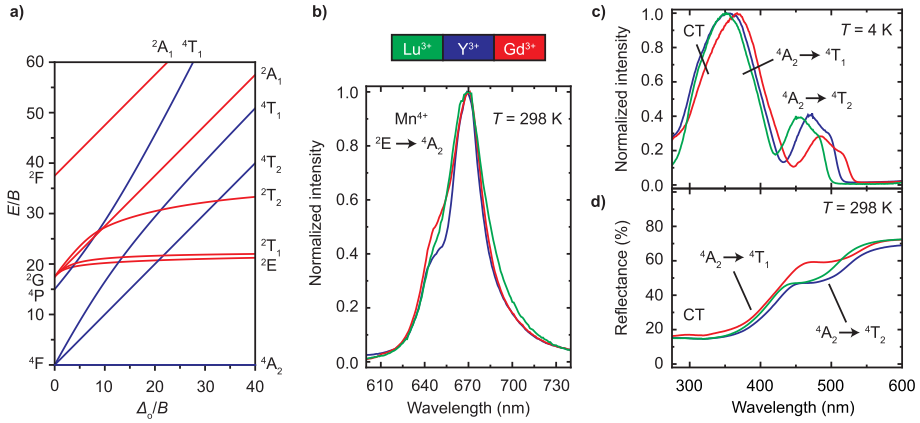

Fig. 2. – **Electronic structure for Mn^{4+} in $RE_2Sn_2O_7$. (a)** Tanabe-Sugano diagram of the d^3 electron configuration in an octahedral crystal field. The doublet and quartet states are shown in red and blue, respectively. **(b)** Room temperature PL spectra of $RE_2Sn_2O_7$:Mn^{4+} (1%) for $RE^{3+} = Gd^{3+}$ (red, $\lambda_{exc} = 350$ nm), Y^{3+} (blue, $\lambda_{exc} = 360$ nm) and Lu^{3+} (green, $\lambda_{exc} = 335$ nm). **(c)** Low temperature ($T = 4$ K) PL excitation spectra of $RE_2Sn_2O_7$:Mn^{4+} (1%) for $RE^{3+} = Gd^{3+}$ (red, $\lambda_{em} = 668$ nm), Y^{3+} (blue, $\lambda_{em} = 665$ nm) and Lu^{3+} (green, $\lambda_{em} = 665$ nm). **(d)** Room temperature diffuse reflectance spectra of $RE_2Sn_2O_7$:Mn^{4+} (1%) for $RE^{3+} = Gd^{3+}$ (red), Y^{3+} (blue) and Lu^{3+} (green). (For interpretation of the references to color in this figure legend, the reader is referred to the web version of this article.)

Table 1
The ionic radius of the eight-coordinated RE^{3+} ion (in Å) and the Mn^{4+}-O^{2-} distance (in Å) of the $RE_2Sn_2O_7$:Mn^{4+} phosphors [20,21].

Pyrochlore	RE^{3+} ionic radius (Å)	Mn^{4+}–O^{2-} distance (Å)
$Lu_2Sn_2O_7$	0.977	2.040
$Y_2Sn_2O_7$	1.019	2.043
$Gd_2Sn_2O_7$	1.053	2.048

symmetry. The splitting of the Mn^{4+} energy levels in a perfect octahedral crystal field is given by the Tanabe-Sugano diagram of the d^3 electron configuration [22], which is displayed in Fig. 2a. The doublet and quartet states are depicted in red and blue, respectively. The Tanabe-Sugano diagram shows that the energies of the levels are strongly dependent on the crystal field strength (Δ_o), except for the ^2E and $^2T_1$ state. Due to its high effective charge, the Mn^{4+} ion experiences a strong crystal field and therefore the ^2E state is generally the lowest energy excited state. Hence, the photoluminescence (PL) spectrum of $RE_2Sn_2O_7$:Mn^{4+} (1%) is dominated by a narrow emission band around 670 nm corresponding to the parity- and spin-forbidden $^2E \rightarrow {}^4A_2$ transition, as can be seen in Fig. 2b. The emission band is narrow as the energy of the ^2E state hardly depends on the crystal field strength and because the ^2E and $^4A_2$ state are both derived from the same t_2^3 electronic configuration.

The low temperature ($T = 4$ K) PL excitation spectra of $RE_2Sn_2O_7$:Mn^{4+} (1%) in Fig. 2c show that the narrow band $^2E \rightarrow {}^4A_2$ emission can be efficiently excited through the $^4A_2 \rightarrow {}^4T_1$ and $^4A_2 \rightarrow {}^4T_2$ transitions. In the spectra we observe two broad intense excitation bands around 350 and 475 nm which are assigned to the spin-allowed $^4A_2 \rightarrow {}^4T_1$ and $^4A_2 \rightarrow {}^4T_2$ transitions, respectively (see also Tanabe-Sugano diagram in Fig. 2a). The trigonal site symmetry (D_{3d}) for Mn^{4+} in $RE_2Sn_2O_7$ causes a splitting of the triplet states ($^4T_1$ and $^4T_2$) into a singlet and doublet state [21,23]. This splitting is clearly visible in the excitation band corresponding to the $^4A_2 \rightarrow {}^4T_2$ transition but not observed for the $^4A_2 \rightarrow {}^4T_1$ transition, probably also because this band has a strong overlap with the broad charge-transfer absorption band (see below).

The intense Mn^{4+} $^4A_2 \rightarrow {}^4T_1$ and $^4A_2 \rightarrow {}^4T_2$ absorption bands are also observed in the room temperature diffuse reflection spectra of the $RE_2Sn_2O_7$:Mn^{4+} (1%) phosphors shown in Fig. 2d. However, the most intense absorption in the diffuse reflection spectra is between 275 and 350 nm, which is assigned to the $O^{2-} \rightarrow Mn^{4+}$ charge-transfer (CT) transition [24]. The relative intensity of the $O^{2-} \rightarrow Mn^{4+}$ CT transition is weaker in the excitation spectra in Fig. 2c, appearing only as a shoulder on the high energy side of the $^4A_2 \rightarrow {}^4T_1$ excitation band. The lower intensity of the $O^{2-} \rightarrow Mn^{4+}$ CT transition in the excitation spectra indicates that excitation into the CT state results in less efficient luminescence than excitation into the Mn^{4+} crystal field states. A large offset of the CT state parabola in the configurational coordinate diagram can explain that excitation in the CT state is followed by direct relaxation to the ground state, competing with relaxation to the emitting ^2E state.

The spectra in Fig. 2c and 2d show that the energies of the $^4T_1$ and $^4T_2$ state depend on the type of RE^{3+} ion in the $RE_2Sn_2O_7$ pyrochlore. Using the data from Table 1 it is found that the energy of the $^4T_1$ and $^4T_2$ state, and therefore the crystal field strength for Mn^{4+}, increases with decreasing Mn^{4+}-O^{2-} distance and RE^{3+} ionic radius, as expected from the electrostatic point charge model. By determining the barycenter energy of the $^4A_2 \rightarrow {}^4T_2$ excitation bands in Fig. 2c, it is estimated that the crystal field strength 10 Dq of Mn^{4+} in $RE_2Sn_2O_7$ varies from 20,234 cm^{-1} for $RE^{3+} = Gd^{3+}$ to 21,521 cm^{-1} for $RE^{3+} = Lu^{3+}$. A more detailed investigation of the crystal field strength for Mn^{4+} and other impurity ions in stannate pyrochlores can be found in Refs. [13,25].

3.3. *Vibronic structure of the Mn^{4+} $^2E \rightarrow {}^4A_2$ luminescence*

In $RE_2Sn_2O_7$ the Mn^{4+} ions are situated on a D_{3d} site with inversion symmetry. Due to the inversion symmetry, the transition between the Mn^{4+} ^2E and $^4A_2$ state responsible for the red luminescence of $RE_2Sn_2O_7$:Mn^{4+} (see Fig. 2b) is both parity- and spin-forbidden. The electronic transition however gains intensity by coupling to vibronic modes that induce odd-parity crystal field terms that allow admixture of opposite parity states into the ^2E and $^4A_2$ states, and thereby make the transition partly allowed for electric dipole radiation. To investigate which vibronic modes couple to the $^2E \rightarrow {}^4A_2$ transition for Mn^{4+} in $RE_2Sn_2O_7$, we studied the luminescence of $RE_2Sn_2O_7$:Mn^{4+} at temperatures down to 4 K. Fig. 3a shows the PL spectrum of $Y_2Sn_2O_7$:Mn^{4+} (1%) at various temperatures between room temperature and 4 K. Upon cooling to cryogenic temperatures, sharp peaks emerge which correspond to the various Stokes and anti-Stokes vibronic electric dipole $^2E \rightarrow {}^4A_2$ transitions. At 4 K all anti-Stokes emission lines have disappeared and the emission spectrum consists of the purely electronic

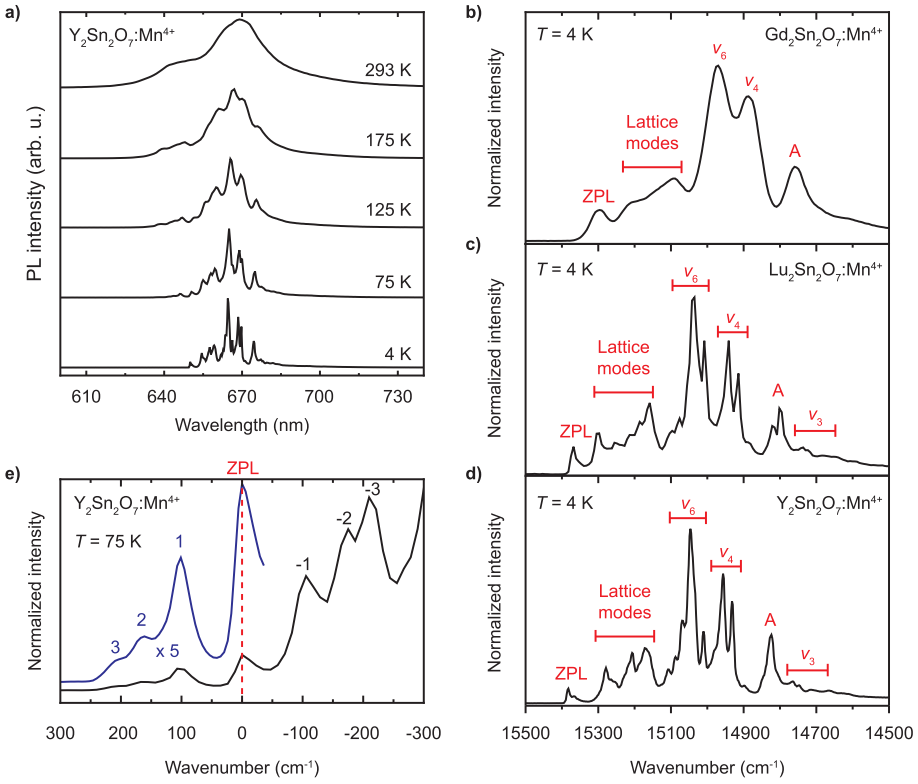

Fig. 3. – Vibronic structure of the Mn^{4+} $^2E \rightarrow {}^4A_2$ luminescence of $RE_2Sn_2O_7:Mn^{4+}$. **(a)** PL spectra of $Y_2Sn_2O_7:Mn^{4+}$ (1%) measured in the range of $T = 4$–293 K for $\lambda_{exc} = 360$ nm. **(b)-(d)** High-resolution PL spectra of $RE_2Sn_2O_7:Mn^{4+}$ (1%) at $T = 4$ K, with **(b)** $RE^{3+} = Gd^{3+}$; $\lambda_{exc} = 485$ nm, **(c)** $RE^{3+} = Lu^{3+}$; $\lambda_{exc} = 351$ nm and **(d)** $RE^{3+} = Y^{3+}$; $\lambda_{exc} = 470$ nm. The peaks corresponding to the zero-phonon line (ZPL) and vibronic sidebands of the $^2E \rightarrow {}^4A_2$ transition are indicated by the red labels. **(e)** PL spectra of the zero-phonon line (ZPL), anti-Stokes and Stokes emission lines of $Y_2Sn_2O_7:Mn^{4+}$ (1%) at $T = 75$ K ($\lambda_{exc} = 360$ nm). The energies of the anti-Stokes and Stokes emission lines are shown relative to the energy of the zero-phonon transition. (For interpretation of the references to color in this figure legend, the reader is referred to the web version of this article.)

transition (zero-phonon line; ZPL) and several vibronic $^2E \rightarrow {}^4A_2$ emission lines on the low-energy side of the ZPL transition.

Fig. 3b–d shows low-temperature ($T = 4$ K) high resolution PL spectra of the $^2E \rightarrow {}^4A_2$ luminescence of Mn^{4+} in $Gd_2Sn_2O_7$ (Fig. 3b), $Lu_2Sn_2O_7$ (Fig. 3c) and $Y_2Sn_2O_7$ (Fig. 3d). For all three $RE_2Sn_2O_7:Mn^{4+}$ phosphors the emission spectrum at 4 K consists of a group of narrow emission lines which correspond to the ZPL and vibronic sidebands of the $^2E \rightarrow {}^4A_2$ transition. However, a striking difference is that the emission lines in the spectrum of $Gd_2Sn_2O_7:Mn^{4+}$ are much broader and show less resolved vibronic structure than the emission lines in the spectra of the other $RE_2Sn_2O_7:Mn^{4+}$ phosphors.

The vibronic structure of the $^2E \rightarrow {}^4A_2$ luminescence at 4 K is expected to be similar for the three $RE_2Sn_2O_7:Mn^{4+}$ phosphors as the crystal structure of the stannate pyrochlores and the site symmetry of the Mn^{4+} (Sn^{4+}) ions are identical [21]. Hence, it surprising that the emission lines are broader for $Gd_2Sn_2O_7:Mn^{4+}$. The significant inhomogeneous broadening indicates that more disorder is present in the MnO_6 octahedrons for Mn^{4+} in $Gd_2Sn_2O_7$ compared to the other (Y and Lu) stannate pyrochlores. The disorder can be related to the larger Sn^{4+}-O^{2-} distance in $Gd_2Sn_2O_7$ (see Table 1). There is a significant difference between the ionic radii of Sn^{4+} (0.69 Å) and Mn^{4+} (0.53 Å) ions in six-fold coordination. This difference in size can result in small geometric distortions in the MnO_6 octahedron when Mn^{4+} substitutes for the larger Sn^{4+} in $RE_2Sn_2O_7$. This geometric distortion may be more pronounced in $Gd_2Sn_2O_7$ as this lattice has the largest site for Sn^{4+}.

The highest energy emission line in the spectra at 4 K is assigned to the zero-phonon transition between the ^2E and $^4A_2$ states, labeled ZPL in Fig. 3b–d. The energies of the ZPL, and thus the energies of the ^2E level, are 15,296 cm^{-1} (Gd^{3+}), 15,368 cm^{-1} (Lu^{3+}) and 15,382 cm^{-1} (Y^{3+}), respectively.

The energy of the ^2E level for Mn^{4+} in $RE_2Sn_2O_7$ is in good agreement with the ^2E level energy typically observed for Mn^{4+} in oxides [10]. The ^2E level energies of the $RE_2Sn_2O_7:Mn^{4+}$ phosphors are however relatively high when compared to most other oxides, which increases their potential as red-emitting phosphor for (lighting) applications. The ZPLs have a low intensity relative to the vibronic emission lines as the zero-phonon transition is forbidden for electric dipole radiation due to the inversion symmetry of the D_{3d} site. Hence, only the magnetic dipole $^2E \rightarrow {}^4A_2$ zero-phonon transition is allowed, which has an order of magnitude weaker oscillator strength than the electric dipole zero-phonon transition [23,26].

The results show the type of RE^{3+} cation in the second coordination sphere has an influence on the energy of the ^2E level, in agreement with the results observed for Mn^{4+} in the M_2SiF_6 (M = Na, K, Rb and Cs) compounds [16–19]. The energy differences between the ^2E levels of the $RE_2Sn_2O_7:Mn^{4+}$ phosphors are however small as the energy of the ^2E state, in contrast to the $^4T_1$ and $^4T_2$ states, does not depend on the crystal field strength and is mainly determined by the local covalency (see also Fig. 2a). Consequently, it is observed that the energy of the ^2E level does not increase with decreasing RE^{3+} ion size like the energy of the $^4T_1$ and $^4T_2$ excited states (see Section 3.2 and Table 1). It is interesting to compare the observed trend in the ^2E energy with density functional theory (DFT) calculations for the ^2E level energy of Mn^{4+} in $RE_2Sn_2O_7$ [27]. According to these DFT calculations, the Mn^{4+} ^2E state will have the highest energy when $RE^{3+} = Lu^{3+}$, followed by Gd^{3+} and Y^{3+}. The experimental results in this work however show the energy E of the

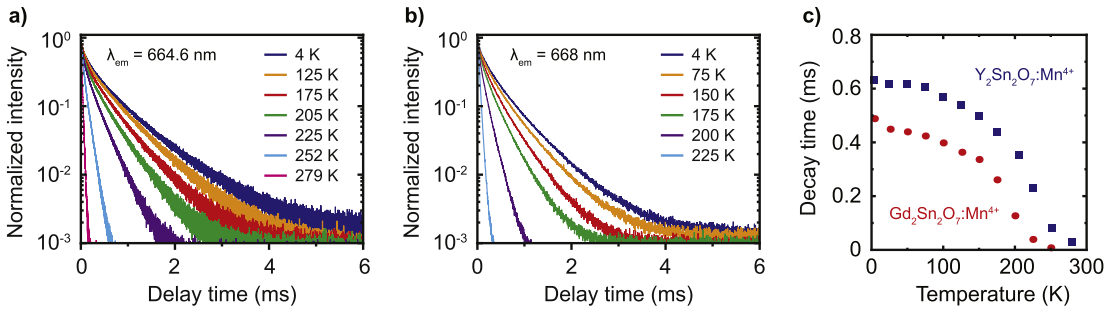

Fig. 4. – PL decay of the Mn^{4+} $^2E \rightarrow {}^4A_2$ luminescence as a function of temperature. PL decay curves of the Mn^{4+} ^2E excited state at various temperatures of **(a)** $Y_2Sn_2O_7:Mn^{4+}$ (1%); $\lambda_{exc} = 470$ nm and $\lambda_{em} = 664.6$ nm, and **(b)** $Gd_2Sn_2O_7:Mn^{4+}$ (1%); $\lambda_{exc} = 485$ nm and $\lambda_{em} = 668$ nm. **(c)** Average PL decay time of the Mn^{4+} ^2E excited state of $Y_2Sn_2O_7:Mn^{4+}$ and $Gd_2Sn_2O_7:Mn^{4+}$ as a function of temperature.

^2E level follows the trend $E(Y^{3+}) > E(Lu^{3+}) > E(Gd^{3+})$, and the highest energy is observed in $Y_2Sn_2O_7:Mn^{4+}$ for which the lowest ZPL energy was predicted. This indicates that a theoretical prediction of transition energies remains challenging.

We now proceed to discuss the more intense vibronic induced $^2E \rightarrow {}^4A_2$ emission lines on the low-energy side of the ZPLs. According to group theory there are six fundamental vibrational modes for an octahedron with O_h symmetry: ν_1 (A_{1g}), ν_2 (E_g), ν_3 (T_{1u}), ν_4 (T_{1u}), ν_5 (T_{2g}), ν_6 (T_{2u}) [23,28]. The Mn^{4+} ^2E and $^4A_2$ state both have even (*gerade*) symmetry and therefore the parity selection rule for electric dipole radiation is only relaxed if the $^2E \rightarrow {}^4A_2$ transition couples with lattice vibrations that are antisymmetric (*ungerade*), i.e. the ν_3, ν_4 and ν_6 mode. Hence, using the energies determined for the *ungerade* modes of the SnO_6 octahedron in $RE_2Sn_2O_7$ [29–31], we assign the most intense vibronic $^2E \rightarrow {}^4A_2$ emission lines in Fig. 3b–d to the ν_6 (~340 cm^{-1} relative to the ZPL) and ν_4 mode (~430 cm^{-1} relative to the ZPL) of the MnO_6 octahedron. The ν_3 mode of the SnO_6 octahedron has an energy of ~650 cm^{-1} and therefore the weak emission peaks around 14,700 cm^{-1} are assigned to this vibronic mode. As the site symmetry of Mn^{4+} $RE_2Sn_2O_7$ is D_{3d} instead of O_h, the triply degenerate ν_3, ν_4 and ν_6 modes split into a double degenerate and single degenerate mode. This splitting is observed in the spectra of $Y_2Sn_2O_7:Mn^{4+}$ (Fig. 3c) and $Lu_2Sn_2O_7:Mn^{4+}$ (Fig. 3d) but not in the spectrum of $Gd_2Sn_2O_7:Mn^{4+}$ (Fig. 3d) where it is probably obscured by the broadening of the emission lines.

Besides the $^2E \rightarrow {}^4A_2$ emission lines induced by coupling to the antisymmetric ν_3, ν_4 and ν_6 modes, several other vibronic $^2E \rightarrow {}^4A_2$ emission lines are observed in Fig. 3b–d. The emission between 15,100 and 15,300 cm^{-1} is assigned to coupling of the $^2E \rightarrow {}^4A_2$ transition with translational or rotational lattice modes involving primarily the metal cations that have been observed between 100 and 250 cm^{-1} [28,31]. Interestingly, an ~180 cm^{-1} mode is found only for Mn^{4+} in the Y-host consistent with the assignment in Ref. [31] to an Y-ion lattice mode at 180 cm^{-1} which is shifted to lower energies in the Gd- and Lu-host because of their higher mass. The emission line located at ~550 cm^{-1} lower energy relative to ZPLs (labeled A) cannot be explained by coupling to anti-symmetric vibrations. We do not have an explanation for what causes this emission line.

To study the vibronic structure of the anti-Stokes $^2E \rightarrow {}^4A_2$ emission, we measured the ZPL and anti-Stokes emission of the $^2E \rightarrow {}^4A_2$ transition of $Y_2Sn_2O_7:Mn^{4+}$ (1%) at $T = 75$ K, which is presented in Fig. 3e (blue line). For comparison, in Fig. 3e we additionally show the Stokes emission with similar energy relative to the ZPL. Three anti-Stokes vibronic sidebands of the $^2E \rightarrow {}^4A_2$ transition (labeled 1 to 3) are observed which are assigned to translational or rotational lattice modes coupling to $^2E \rightarrow {}^4A_2$ transition [28,31]. The anti-Stokes (labeled 1 to 3) and Stokes (labeled −1 to −3) vibronic emission lines are observed at similar energy relative to the ZPL, indicating that similar types of vibrational motions in the ^2E and $^4A_2$ state are responsible for these emission lines. A detailed investigation however reveals that the energy relative to the ZPL is around 15 cm^{-1} smaller for the anti-Stokes emission lines than for the Stokes emission lines. This indicates that the energy of the vibrational modes in the ^2E excited state is slightly lower than in the $^4A_2$ ground state.

3.4. Quenching of the Mn^{4+} $^2E \rightarrow {}^4A_2$ luminescence

For application of Mn^{4+}-doped materials as deep red luminescent materials, the quenching temperature of the emission is an important parameter. Both the emission intensity and luminescence decay time can be measured as a function of temperature to provide insight in the quenching temperature [1,23]. To study the thermal quenching of the $^2E \rightarrow {}^4A_2$ luminescence for $RE_2Sn_2O_7:Mn^{4+}$, here we measured the PL decay of the Mn^{4+} ^2E state as a function of temperature. Fig. 4a and 4b show PL decay curves of the Mn^{4+} ^2E state at various temperatures for $Y_2Sn_2O_7:Mn^{4+}$ (1%) and $Gd_2Sn_2O_7:Mn^{4+}$ (1%). For both phosphors the low temperature PL decay is on the order of a millisecond, which is expected as the transition from the ^2E state to the $^4A_2$ state is both parity- and spin-forbidden. The multi-exponential character of the PL decay (even down to 4 K) indicates that not all Mn^{4+} centers have the same decay time, which is unexpected based on the fact that there is a single crystallographic Sn^{4+} site for which Mn^{4+} substitutes. The non-exponential character may be due to differences in the local coordination of Mn^{4+} that affect the radiative and/or non-radiative decay rate. Because of the strongly forbidden character of the ^2E emission, a small variation in the local surroundings can result in a change of emission decay time explaining the non-exponential character. Because of thermally-activated non-radiative relaxation pathways, the PL decay becomes much faster with increasing temperature and as a result the luminescence is almost fully quenched at room temperature. This is clearly observed in Fig. 4c, which displays the average PL decay time of $Y_2Sn_2O_7:Mn^{4+}$ and $Gd_2Sn_2O_7:Mn^{4+}$ as a function of temperature. The average PL decay time (τ_{avg}) of each decay curve was determined using $\tau_{avg} = \sum I_i t_i / \sum I_i$. The results in Fig. 4c show that the PL decay time is relatively constant up to 100 K. The small initial decrease in decay time can be explained by the temperature dependence of the vibronic transition probabilities, which scale with the phonon occupation number n for anti-Stokes vibronics and $(1 + n)$ for Stokes vibronics. Above 100 K a rapid decrease in emission lifetime is observed until it reaches the μs range above 250 K, indicating strong thermal quenching of the emission. This is confirmed by intensity measurements which show a very weak Mn^{4+} luminescence at room temperature. Similar luminescence

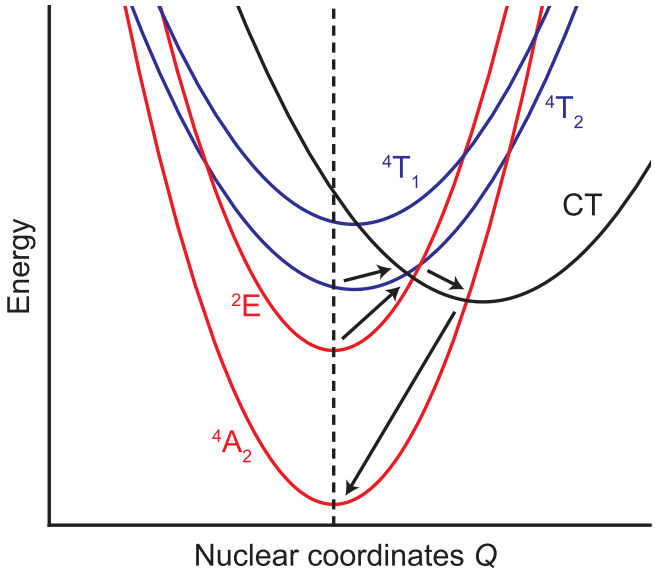

Fig. 5. Configuration coordinate diagram showing the luminescence quenching mechanism proposed for Mn^{4+} in $RE_2Sn_2O_7$.

quenching behavior was observed for $Lu_2Sn_2O_7$:Mn^{4+}.

Strong thermal quenching of Mn^{4+} luminescence below room temperature has previously e.g. been observed for $CaZrO_3$:Mn^{4+} and $CaAl_4O_7$:Mn^{4+} [32,33]. For $CaAl_4O_7$:Mn^{4+} the quenching was assigned to thermally activated crossover from the ^2E excited state to the $^4A_2$ ground state [33]. Since the parabola for the ^2E excited state and $^4A_2$ ground state are at the same equilibrium position (evidenced by sharp line emission) direct crossover is not possible. Only crossover via a third state with a large off-set can explain thermal quenching. For $CaZrO_3$:Mn^{4+}, Blasse et al. assigned the absence of Mn^{4+} luminescence at room temperature to thermally activated crossover involving a low-lying $O^{2-} \rightarrow Mn^{4+}$ charge-transfer (CT) state (CT transition at ~30,000 cm^{-1}) [1,32]. The PL excitation and diffuse reflection spectra of $RE_2Sn_2O_7$:Mn^{4+} in Fig. 2b and 2c showed that the $O^{2-} \rightarrow Mn^{4+}$ CT transition of Mn^{4+} in $RE_2Sn_2O_7$ is relatively low in energy (~30,000 cm^{-1}) and close to the $^4T_1$ crystal field state. Hence, we ascribe the thermal quenching observed for $RE_2Sn_2O_7$:Mn^{4+} to a low-lying $O^{2-} \rightarrow Mn^{4+}$ CT state.

The configuration coordinate diagram in Fig. 5 explains how the low-lying CT state causes quenching of the Mn^{4+} luminescence. Due to the low energy and large offset of the CT state (black parabola), thermal activation over a relatively low barrier already allows crossover from the $^4T_1$ and ^2E state to the CT state, which will be followed by non-radiative relaxation to the ground state via the crossing of the CT and $^4A_2$ parabola. As a consequence of this process (indicated by the arrows in Fig. 5), the Mn^{4+} luminescence is quenched by the increasing thermal energy available at higher temperatures. When the $O^{2-} \rightarrow Mn^{4+}$ CT state is higher in energy the quenching depicted in Fig. 5 only occurs far above room temperature. For example, the commerial Mn^{4+}-activated magnesium fluorogermanate phosphor has a quenching temperature of 700 K in agreement with the higher energy position of the $O^{2-} \rightarrow Mn^{4+}$ CT transition, located at ~35,000 cm^{-1} [1,2].

4. Conclusions

Red emitting Mn^{4+}-doped crystalline materials have potential for application in light emitting devices (lamps, displays) and therefore it is important to understand how the spectroscopic properties of Mn^{4+} are influenced by the host lattice in which the Mn^{4+} ions are situated. Here we investigated the luminescence of three isostructural $RE_2Sn_2O_7$:Mn^{4+} (RE^{3+} = Y^{3+}, Lu^{3+} or Gd^{3+}) phosphors and compared the spectroscopic properties of Mn^{4+} in these three stannate pyrochlores. By measuring PL emission and excitation spectra of $RE_2Sn_2O_7$:Mn^{4+} at cryogenic temperatures, it was determined that the energies of the Mn^{4+} $^4T_1$ and $^4T_2$ states significantly increase with decreasing Mn^{4+}-O^{2-} distance which is explained by an increase in crystal field splitting. The energy of the ^2E state of Mn^{4+} shows a small shift to higher energies from Gd to Lu to Y. The observed shift is not in line with theoretical calculations reported previously. The vibronic structure of the Mn^{4+} luminescence revealed that asymmetrical vibronic modes couple to the $^2E \rightarrow {}^4A_2$ transition. Surprisingly, the low temperature spectra of $Gd_2Sn_2O_7$:Mn^{4+} showed relatively broad emission lines indicating more local disorder for Mn^{4+} in $Gd_2Sn_2O_7$ compared to the other two host lattices. Furthermore, we measured the PL decay of the Mn^{4+} ^2E state as a function of temperature to investigate the thermal quenching behavior for Mn^{4+} in $RE_2Sn_2O_7$, which is an important parameter for applications. The PL decay measurements showed that the luminescence of $RE_2Sn_2O_7$:Mn^{4+} is strongly quenched below room temperature which is explained by relaxation via a low-lying $O^{2-} \rightarrow Mn^{4+}$ charge-transfer state.

Acknowledgements

This work is financially supported by Technologiestichting STW, which is part of the Nederlandse Organisatie voor Wetenschappelijk Onderzoek (NWO).

References

[1] G. Blasse, B.C. Grabmaier, Luminescent Materials, Springer-Verlag, Heidelberg, 1994.
[2] W.M. Yen, S. Shionoya, H. Yamamoto, Phosphor Handbook, 2nd ed., CRC Press, Boca Rotan, 2007.
[3] C.C. Lin, A. Meijerink, R.-S. Liu, Critical red components for next generation white LEDs, J. Phys. Chem. Lett. 7 (2016) 495–503.
[4] E.V. Radkov, L.S. Grigorov, A.A. Setlur & A.M. Srivastava, Red line emitting phosphor materials for use in LED applications, United States patent application US7497973 B2 (2009).
[5] T. Murata, T. Tanoue, M. Iwasaki, K. Morinaga, T. Hase, Fluorescence properties of Mn^{4+} in $CaAl_{12}O_{19}$ compounds as red-emitting phosphor for white LED, J. Lumin. 114 (2005) 207–212.
[6] M. Noginov, G.B. Loutts, Spectroscopic studies of Mn^{4+} ions in yttrium orthoaluminate, J. Opt. Soc. Am. B 16 (1999) 3–11.
[7] G.B. Loutts, et al., Manganese-doped yttrium orthoaluminate: a potential material for holographic recording and data storage, Phys. Rev. B 57 (1998) 3706–3709.
[8] Y. Zhydachevskii, A. Durygin, A. Suchocki, A. Matkovskii, D. Sugak, P. Bilski, S. Warchol, Mn-doped $YAlO_3$ crystal: a new potential TLD phosphor, Nucl. Instr. Meth. Phys. Res. B 227 (2005) 545–550.
[9] Y. Li, Y.-Y. Li, K. Sharafudeen, G.-P. Dong, S.-F. Zhou, Z.-J. Ma, M.-Y. Peng, J.-R. Qiu, A strategy for developing near infrared long-persistent phosphors: taking $MAlO_3$:Mn^{4+},Ge^{4+} (M = La, Gd) as an example, J. Mater. Chem. C 2 (2014) 2019–2027.
[10] M.G. Brik, S.J. Camardello, A.M. Srivastava, Influence of covalency on the Mn^{4+} ^2E_g -> $^4A_{2g}$ emission energy in crystals, ECS J. Solid State Sci. Technol. 4 (2015) R39–R43.
[11] R. Hoshino, S. Adachi, Photo-induced degradation and thermal decomposition in $ZnSnF_6 \cdot 6H_2O$: Mn^{4+} red-emitting phosphor, Opt. Mater. 48 (2015) 36–43.
[12] M.G. Brik, A.M. Srivastava, On the optical properties of the Mn^{4+} ion in solids, J. Lumin 133 (2013) 69–72.
[13] A.M. Srivastava, M.G. Brik, The dependence of 10 Dq crystal field parameter for Mn^{4+} ($3d^3$ configuration) and the magnitude of $^7F_1$ level splitting for Eu^{3+} ($4f^6$ configuration) on pyrochlore compositions, Opt. Mater. 35 (2012) 196–200.
[14] A.G. Paulusz, Efficient Mn(IV) emission in fluorine coordination, J. Electrochem. Soc. 120 (1973) 942–947.
[15] A.M. Srivastava, M.G. Brik, Crystal field studies of the Mn^{4+} energy levels in the perovskite, $LaAlO_3$, Opt. Mater. 35 (2013) 1544–1548.
[16] S.L. Chodos, A.M. Black, C.D. Flint, Vibronic spectra and lattice dynamics of Cs_2MnF_6 and $A_2M^{IV}F_6$:MnF_6^{2-}, J. Chem. Phys. 65 (1976) 4816–4824.
[17] H.F. Sijbom, J.J. Joos, L.I.D.J. Martin, K. Van den Eeckhout, D. Poelman, P.F. Smet, Luminescent behavior of the K_2SiF_6:Mn^{4+} red phosphor at high fluxes and at the microscopic level, ECS J. Solid State Sci. Technol. 5 (2016) R3040–R3048.

[18] T. Takahashi, S. Adachi, Mn^{4+}-activated red photoluminescence in K_2SiF_6 phosphor, J. Electrochem. Soc. 155 (2008) E183–E188.
[19] Y.K. Xu, S. Adachi, Properties of Na_2SiF_6:Mn^{4+} and Na_2GeF_6:Mn^{4+} red phosphors synthesized by wet chemical etching, J. Appl. Phys. 105 (2009) 013525.
[20] R.D. Shannon, Revised effective ionic radii and systematic studies of interatomic distances in halides and chalcogenides, Acta Cryst. A32 (1976) 751–767.
[21] B.J. Kennedy, B.A. Hunter, C.J. Howard, Structural and bonding trends in tin pyrochlore oxides, J. Solid State Chem. 130 (1997) 58–65.
[22] Y. Tanabe, S. Sugano, On the absorption spectra of complex ions II, J. Phys. Soc. Jpn. 9 (1954) 776–779.
[23] B. Henderson, G.F. Imbusch, Optical Spectroscopy of Inorganic Solids, Clarendon Press, Oxford, 1989.
[24] M.G. Brik, A.M. Srivastava, N.M. Avram, Comparative analysis of crystal field effects and optical spectroscopy of six-coordinated Mn^{4+} ion in the $Y_2Ti_2O_7$ and $Y_2Sn_2O_7$ pyrochlores, Opt. Mater. 33 (2011) 1671–1676.
[25] M.G. Brik, A.M. Srivastava, Comparative crystal field analysis of energy level schemes and nephelauxetic effect for Cr^{4+}, Cr^{3+}, and Mn^{4+} ions in $Y_2Sn_2O_7$ pyrochlore, Opt. Mater. 35 (2013) 1251–1256.
[26] D.F. Nelson, M.D. Sturge, Relation between absorption and emission in the region of the *R* lines of ruby, Phys. Rev. 137 (1965) A1117–A1130.
[27] M.H. Du, Mn^{4+} emission in pyrochlore oxides, J. Lumin. 157 (2015) 69–73.
[28] I.W. Forrest, A.P. Lane, Single-crystal polarized infrared and raman spectra and normal-coordinate analysis of some group 4 complex hexafluorometalates, Inorg. Chem. 15 (1976) 265–269.
[29] A.J.H. Macke, G. Blasse, Vibrational spectra of oxidic stannates in relation to order-disorder phenomena, J. Inorg. Nucl. Chem. 38 (1976) 1409–1411.
[30] M.T. Vandenborre, E. Husson, Comparison of the force field in various pyrochlore families. I. The $A_2B_2O_7$ oxides, J. Solid State Chem. 50 (1983) 362–371.
[31] J.F. McCaffrey, N.T. McDevitt, C.M. Philippi, Infrared lattice spectra of rare-earth stannate and titanate pyrochlores, J. Opt. Soc. Am. 61 (1971) 209–212.
[32] G. Blasse, P.H.M. de Korte, The luminescence of tetravalent manganese in $CaZrO_3$:Mn, J. Inorg. Nucl. Chem. 43 (1981) 1505–1506.
[33] P. Li, M. Peng, X. Yin, Z. Ma, G. Dong, Q. Zhang, J. Qiu, Temperature dependent red luminescence from a distorted Mn^{4+} site in $CaAl_4O_7$:Mn^{4+}, Opt. Express 21 (2013) 18943.